Journal of Computational and Applied Mathematics 386 (2021) 113231

Contents lists available at ScienceDirect

Journal of Computational and Applied Mathematics

journal homepage: www.elsevier.com/locate/cam

A new method of internal auxiliary source-sinks (MIASS) for two-dimensional interior Dirichlet acoustic problems

Yuri A. Eremin [a], George Fikioris [b], Nikolaos L. Tsitsas [c,*], Thomas Wriedt [d]

[a] *Lomonosov Moscow State University, Lenin's Hills, 119991 Moscow, Russia*
[b] *School of Electrical and Computer Engineering, National Technical University of Athens, Athens, Greece*
[c] *School of Informatics, Aristotle University of Thessaloniki, Thessaloniki, Greece*
[d] *Leibniz-Institut für Werkstofforientierte Technologien-IWT, University of Bremen, Bremen, Germany*

ARTICLE INFO

Article history:
Received 6 December 2019
Received in revised form 9 June 2020

MSC:
34K10
31A10
65N38

Keywords:
Interior boundary-value problems
Compact operators
Helmholtz equations
Discrete sources methods

ABSTRACT

A new Method of Internal Auxiliary Source–Sinks (MIASS) is developed for the numerical solution of the two-dimensional interior Dirichlet acoustic problem for the Helmholtz equation. We give two versions of MIASS, one for a closed auxiliary curve (MIASS-C) and another for an open auxiliary curve (MIASS-O). The mathematical and numerical foundations of both versions are provided. In particular, we show that the integral operator that pertains to the associated integral equation has a dense range. We then demonstrate completeness and linear independence of the discrete system of source-sinks. Indicative numerical results are given and numerical implementation aspects are discussed.

1. Introduction

For a region with a smooth boundary, we develop a computational method for the two-dimensional (2-D) interior Dirichlet acoustic problem pertaining to the scalar Helmholtz equation. Our method – to be referred to as the *Method of Internal Auxiliary Source–Sinks (MIASS)* – resembles the well-known Method of Auxiliary Sources (MAS) [1] in that both methods first determine auxiliary quantities generating a solution that is required to satisfy the Dirichlet boundary condition. We introduce two versions of MIASS, called MIASS-C and MIASS-O. The differences between MAS and MIASS-C are two:
(i) The auxiliary quantities in MIASS-C are "source-sinks" as opposed to the sources of the MAS. By "source–sink" we mean a point source together with a collocated point sink, superimposed so that there is no singularity at the source–sink point. We note that the source–sink concept is well known in the literature (see, e.g., [2] and [3], which deal with three-dimensional (3-D) problems), but we use our source-sinks for a different purpose. Mathematically (for the case of two dimensions of interest herein) MIASS-C uses the first-kind Bessel functions (J_0) in place of the Hankel functions ($H_0^{(1)}$) of MAS.
(ii) In both MIASS-C and MAS, the auxiliary quantities lie on a closed curve. Whereas MAS uses an auxiliary curve lying *outside* the region of interest (recall that we are discussing an *interior* problem), in MIASS-C the curve is *inside*.

Our second version, MIASS-O, signals yet two more departures from conventional MAS. The two differences between MIASS-C and MIASS-O are:

* Corresponding author.
E-mail address: ntsitsas@csd.auth.gr (N.L. Tsitsas).

https://doi.org/10.1016/j.cam.2020.113231
0377-0427/

(iii) MIASS-O uses an auxiliary curve Γ that is *open* (instead of the closed auxiliary curve of MIASS-C).
(iv) MIASS-O uses not only the forenamed source-sinks, but also the "source–sink derivatives", by which we mean the normal to Γ derivatives of the aforementioned Bessel functions.

In the present work, we confine ourselves to the 2-D interior Dirichlet problem. Thus, MIASS-C seeks a solution as a superposition of source-sinks, with each source–sink setting up a standing-wave distribution within the 2-D cavity in which the Helmholtz equation is to be solved. However, it is apparent that both MIASS-C and MIASS-O (or variants) can be extended to more complicated boundary-value problems, including transmission problems. Thus, our main purpose is to provide the mathematical and numerical foundations of a method that is expected to prove useful for a number of problems whose domain of interest includes an interior region.

After giving some preliminaries (Section 2) and defining the boundary-value problem we wish to solve, we describe (in Section 3.1) what we call the "continuous version" of MIASS-C. Rather than a system of linear equations for the unknown source–sink coefficients, the continuous version involves an integral equation for an unknown function – called the *density* – that is defined on the auxiliary surface. In Section 4, we show that the integral operator pertaining to this integral equation has a dense range. Sections 5 and 6, which rely on Section 4, demonstrate completeness and linear independence of the (discrete) system of source-sinks. The above sections concern MIASS-C, but re-formulated theorems hold for the aforementioned MIASS-O, as shown in Section 7. Section 8 gives indicative numerical results that agree well with results obtained using MAS; in this section, some numerical-implementation aspects of MIASS are also briefly discussed. Finally, Section 9 proposes future work that can shed further light on the advantages and disadvantages of MIASS.

The results in Sections 4–6 are similar to results in other works pertaining to complete sets of solutions to the Helmholtz equation, most notably the pioneering work of Kupradze [4]. Indeed, there are many such complete solutions sets, so that the pertinent literature is vast (see, e.g. [5–9]). The complete set that is perhaps closest to our own is the set of entire functions on pp. 49 and 52 of [5]—however, this set is relevant to 3-D problems.

Our MIASS can be viewed as a particular instance of a family of methods, usually called the Discrete Sources Methods (DSMs). The first version of the DSMs was published in 1980 [10]. It was limited to problems of electromagnetic scattering by perfect conductors under axial excitation (i.e., a plane wave propagating along an axis of symmetry); this simple excitation allowed one to construct the approximate solution as a combination of electric and magnetic dipoles lying on the axis of symmetry. In 1982, the method was extended to a homogeneous penetrable obstacle [11]; this was the first time regular (Bessel) functions were used to represent the field inside a penetrable scatterer. The 1983 work [12] is a theoretical treatment of DSMs. The first version of DSMs had some limitations associated with obstacle geometry, as it was not able to analyze an obstacle that is oblate. This was overcome in 1983 by means of analytic continuation for the support of the discrete sources (DSs) into a complex plane adjoining the symmetry axis of the obstacle [13]. Placing the DSs on this complex plane eliminated the limitations of the original DSM scheme and enabled treatment of more general obstacle geometries. In 1985, the DSM was generalized to analyze non-axial excitations of an axial symmetric particle [14]. Theoretical outlines of DSMs along with a generic scheme that allowed generation of complete systems based on DSs supports came in 1987, while some new complete systems of DSs for the Helmholtz and the Maxwell equations were introduced in [15]. Another modification, proposed in 1993, allowed taking into consideration not only the axial symmetry of the obstacle, but also the polarization of the exciting field [16]. Later editions of the DSMs had the benefit of expanding the technique to practical applications; see, e.g., [17]. Further information on the DSMs family can be found in chapter IV of [5].

2. Notation and preliminaries

Our notation is similar to that of Colton and Kress [18,19]. The symbols D and G denote bounded open regions in $\mathbb{R}^2$. We denote closures by $\overline{D}$ and $\overline{G}$ and boundaries by ∂D and ∂G. Thus, the exteriors are $\mathbb{R}^2 \setminus \overline{D}$ and $\mathbb{R}^2 \setminus \overline{G}$. The symbols x and y always denote points in $\mathbb{R}^2$, or in specified subsets of $\mathbb{R}^2$.

We proceed to summarize some well-known results that we will use throughout.

2.1. Addition theorems

We use two addition theorems involving the cylindrical Bessel and Hankel functions $J_m(z)$ and $H_m^{(1)}(z)$ (see p. 101, Eqs. (29) and (31) of [20]). The first is

$$H_0^{(1)}\left(\sqrt{z_1^2+z_2^2-2z_1z_2\cos\theta}\right) = \sum_{m=-\infty}^{\infty} J_m(z_1)H_m^{(1)}(z_2)e^{\mathrm{i}m\theta}, \tag{1}$$

where $\theta \in \mathbb{R}$ and $z_1, z_2 \in \mathbb{C}$ with $|z_1| < |z_2|$. The second is

$$J_0\left(\sqrt{z_1^2+z_2^2-2z_1z_2\cos\theta}\right) = \sum_{m=-\infty}^{\infty} J_m(z_1)J_m(z_2)e^{\mathrm{i}m\theta}, \tag{2}$$

where $\theta \in \mathbb{R}$ and $z_1, z_2 \in \mathbb{C}$. Since ([21], §10.19)

$$J_m(z) \sim \frac{1}{\sqrt{2\pi m}}\left(\frac{ez}{2m}\right)^m \quad (m \to +\infty, \quad z \neq 0), \tag{3}$$

and

$$H_m^{(1)}(z) \sim -\mathrm{i}\sqrt{\frac{2}{\pi m}}\left(\frac{ez}{2m}\right)^{-m} \quad (m \to +\infty, \quad z \neq 0), \tag{4}$$

the terms of the series on the right-hand side of (1) behave like $(z_1/z_2)^{|m|}/|m|$ for large $|m|$, so that the series converges rapidly. The series in (2) converges even faster.

2.2. Dirichlet Problems for the Helmholtz equation; uniqueness theorems

The 2-D scalar Helmholtz equation is

$$\Delta u(x) + k^2 u(x) = 0, \tag{5}$$

where Δ is the Laplace operator and the sign of $k \in \mathbb{C}$ is chosen so that

$$\operatorname{Im} k \geq 0. \tag{6}$$

For a C^2 boundary ∂D, the Dirichlet boundary condition is

$$u(x) = f(x), \quad x \in \partial D, \tag{7}$$

where $f(x)$ is a given continuous function.

When (5) holds for x in a region D that is bounded, then the *interior Dirichlet problem* consists of Eq. (5) (for $x \in D$) together with the boundary condition (7). This problem has a unique continuous solution provided that D is non-resonant, meaning that k is not an interior Dirichlet eigenvalue for D (pp. 75–78 and p. 107 of [18]). The said eigenvalues are real and positive and accumulate only at infinity.

When (5) holds for x in the unbounded region $\mathbb{R}^2 \setminus \overline{D}$, then the *exterior Dirichlet problem* consists of (5) and (7) together with the Sommerfeld radiation condition at infinity, viz.,

$$\lim_{\rho\to\infty} \sqrt{\rho}\left(\frac{\partial u}{\partial \rho} - \mathrm{i}ku\right) = 0, \quad \rho = |x|. \tag{8}$$

This problem always has a unique continuous solution (p. 76 and p. 83 of [18]).

2.3. Single-layer potential

Let ∂D be a bounded closed curve in $\mathbb{R}^2$ with $\partial D \in C^{2,\alpha}$, where $C^{2,\alpha}$ is the usual Hölder space of α-continuous functions ($0 < \alpha \leq 1$). Let $g(x)$, the *density*, be a $L_2(\partial D)$ function. The 2-D acoustic *single-layer potential* $q(y)$ is the line integral (p. 39 and p. 66 of [19])

$$q(y) = \frac{\mathrm{i}}{4}\int_{\partial D} H_0^{(1)}(k|x-y|)\, g(x)\, \mathrm{d}s_x, \quad y \in \mathbb{R}^2 \setminus \partial D. \tag{9}$$

We use the following properties of $q(y)$.
(i) $q(y)$ satisfies the Helmholtz equation in the interior D (p. 39 of [19]).
(ii) $q(y)$ satisfies the Helmholtz equation in the exterior $\mathbb{R}^2 \setminus \overline{D}$ (p. 39 of [19]).
(iii) $q(y)$ is analytic in both the interior and the exterior of ∂D (p. 46 and p. 72 of [18]).
(iv) $q(y)$ is continuous across ∂D (p. 45 of [19]).
(v) The normal to ∂D derivative of $q(y)$ satisfies the jump relation (p. 45 of [19])

$$\lim_{\delta\to 0}\left[\frac{\partial q(y+\nu\delta)}{\partial \nu} - \frac{\partial q(y-\nu\delta)}{\partial \nu}\right] = -g(y), \quad \text{almost everywhere on } \partial D, \tag{10}$$

in which the first (second) term denotes the interior (exterior) normal derivative.
(vi) $q(y)$ satisfies the Sommerfeld radiation condition (8) at $y = \infty$ (p. 39 of [19]).

We now describe the problem we wish to solve.

3. Statement of problem; continuous version of MIASS-C

Our purpose is to develop a computational method for the following 2-D acoustic problem.

Let $\partial D \in C^{2,\alpha}$. With an $e^{-\mathrm{i}\omega t}$ time dependence ($\omega > 0$) assumed and suppressed, we seek a velocity potential $u(x) \in C^2(D) \cap C(\overline{D})$ that satisfies the interior Dirichlet problem

$$\Delta u(x) + k^2 u(x) = 0, \quad x \in D; \qquad u(x) = f(x), \ x \in \partial D; \quad \operatorname{Im} k \geq 0, \tag{11}$$

where $f(x) \in C(\partial D)$ and $k = \sqrt{\omega(\omega + \mathrm{i}\gamma)/c^2}$, where $\gamma > 0$ and $c > 0$ are, respectively, the damping coefficient and the speed of sound within D [22]. Throughout this paper, we assume that ∂D is non-resonant in the sense discussed in Section 2.2. We call ∂D the *physical closed curve.*

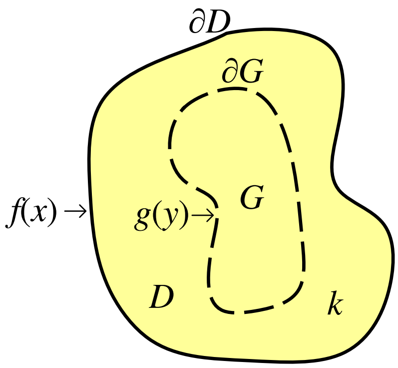

Fig. 1. The considered 2-D interior Dirichlet problem. Shown are the physical closed curve ∂D together with an auxiliary closed curve ∂G used for the application of MIASS-C.

3.1. Continuous version of MIASS-C

Now let G be a bounded and open region with boundary $\partial G \in C^{2,\alpha}$, which we assume throughout to be non-resonant. We also assume that $G \subsetneqq D$, i.e. G is a proper subset of D; see Fig. 1. We call ∂G the *auxiliary closed curve*.

For any $g(y) \in L_2(\partial G)$ (we call $g(y)$ the *density*), define $u_g(x)$ by means of the line integral

$$u_g(x) = \int_{\partial G} J_0(k|x-y|)\, g(y)\, \mathrm{d}s_y, \quad x \in D. \tag{12}$$

The function $u_g(x)$ is continuous for any L_2-function $g(y)$.

For any fixed $y \in \partial G$, the kernel $J_0(k|x-y|)$ satisfies the Helmholtz equation (5) with respect to $x \in D$. Furthermore, for any $g(y)$, we can differentiate (12) under the integral sign. Therefore, $u_g(x)$ also satisfies the Helmholtz equation (5) for any choice of $g(y)$. Moreover, if the density $g(y)$ is such that the integral equation

$$\int_{\partial G} J_0(k|x-y|)\, g(y)\, \mathrm{d}s_y = f(x), \quad x \in \partial D \tag{13}$$

is satisfied, then $u_g(x)$ possesses the additional property of satisfying the boundary condition (7). Consequently, the continuous function $u_g(x)$, defined via (12) and (13), is the unique continuous solution to our interior Dirichlet problem (11).

The process we just described – which can be called the *continuous version of MIASS-C* – consists of solving the linear, first-kind Fredholm integral equation (13) for the density $g(y)$, and then finding $u_g(x)$ from (12).

The interpretation in terms of source-sinks (see Introduction) follows from the identity

$$J_0(k|x-y|) = \frac{1}{2}\left[H_0^{(1)}(k|x-y|) + H_0^{(2)}(k|x-y|)\right], \tag{14}$$

because, under the considered $e^{-\mathrm{i}\omega t}$ time dependence, the first (second) Hankel function represents an outgoing (incoming) wave, tantamount to a source (sink) located at y. In (14), the source–sink superposition is such that there is no singularity when $x = y$. Eq. (12) thus seeks $u(x)$ as a superposition of nonsingular source-sinks, each located at $y \in \partial G$ and weighted by $g(y)$. By contrast, the continuous version of the MAS (i.e. the continuous version of the conventional Method of Auxiliary Sources; see chapt. 5 of [1] and [23]) uses sources/Hankel functions (rather than source-sinks/Bessel functions) and an exterior (rather than an interior) auxiliary closed curve.

3.2. Integral operator and its range

Let us define a linear operator $\mathbf{K} : L_2(\partial G) \to L_2(\partial D)$ associated with the left-hand side of the integral equation (13), so that

$$(\mathbf{K}g)(x) = \int_{\partial G} J_0(k|x-y|)\, g(y)\, \mathrm{d}s_y. \tag{15}$$

Evidently (p. 300 and p. 352 of [24]), $J_0(k|x-y|)$ is a Hilbert–Schmidt kernel and $\mathbf{K}$ is a Hilbert–Schmidt operator. Therefore (p. 353 of [24]), $\mathbf{K}$ is a compact operator.

In infinite-dimensional spaces, operator compactness has well-known consequences pertaining to existence, uniqueness, and/or stability (see, e.g., pp. 36–37 and pp. 85–87 of [19]): A compact operator $\mathbf{K}$ may not be injective, or may not be surjective; even when $\mathbf{K}$ is invertible, the inverse $\mathbf{K}^{-1}$ (defined on the range $R(\mathbf{K})$ of $\mathbf{K}$) is necessarily unbounded

(p. 336 of [24]); the range $R(\mathbf{K})$ of a compact $\mathbf{K}$ is typically "small"; and the associated first-kind Fredholm integral equation is, for a given right-hand side, unlikely to have a solution.

In other words, given an L_2-right-hand-side $f(x)$, an L_2-solution $g(y)$ of the integral equation (13) will, in general, not exist; cf. pp. 36–37 of [19]. For the $\mathbf{K}$ defined in (15), the question now arises: How "small" is $R(\mathbf{K})$? We can get an idea by considering the special case where both $\overline{G}$ and $\overline{D}$ are circular discs. In this special case, $\mathbf{K}$ is a 2π-convolution operator and can be explicated using Fourier series as follows.

Let ∂D and ∂G be circles of radii b and a $(b > a)$, respectively, and let $x \in \partial D$ and $y \in \partial G$ have polar coordinates (b, ϕ_x) and (a, ϕ_y), with $0 \leq \phi_x, \phi_y < 2\pi$. Since $k|x-y| = k\sqrt{a^2+b^2-2ab\cos(\phi_x-\phi_y)}$ with $|ka| < |kb|$, we can apply the addition theorem (2) to the Bessel function appearing on the left-hand side of (15). If $\sum_{m=-\infty}^{\infty} g_m \exp(im\phi_y)$ denotes the Fourier series of the ϕ_y-dependent function $g(y)$, we see that (15) reduces to

$$(\mathbf{K}g)(x) = 2\pi a \sum_{m=-\infty}^{\infty} g_m J_m(ka) J_m(kb) \exp(im\phi_x). \tag{16}$$

Because of (3), the Fourier-series coefficients $g_m J_m(ka) J_m(kb)$ of the ϕ_x-dependent function $(\mathbf{K}g)(x)$ are much smaller than g_m when $|m|$ is large. Thus, any element $(\mathbf{K}g)(x)$ belonging to $R(\mathbf{K})$ possesses a Fourier series whose coefficients decay much more rapidly than those of $g(y)$. Since $g(y)$ is an arbitrary element of $L_2(\partial G)$, the range $R(\mathbf{K})$ is much smaller than $L_2(\partial D)$. Note the intimate connection of the "smallness" to the rapidity of convergence of the series in the addition theorem; note also that (3) can be used to accurately describe the range.

For the case of MIASS-C, actual numerical problems associated with the aforementioned general difficulties will be described in Section 8. In the meantime, we proceed to show that $R(\mathbf{K})$, however small, is dense.

4. Integral operator of MIASS-C: Density of range

We now show that the compact (and thus bounded) linear operator $\mathbf{K}$ defined in (15) has a range that is dense in $L_2(\partial D)$. In our proof, an important role is played by a certain homogeneous Dirichlet problem involving the adjoint operator $\mathbf{K}^*$.

Theorem 1. *Let G and D be non-resonant regions of $\mathbb{R}^2$ with $\partial G \in C^{2,\alpha}$, $\partial D \in C^{2,\alpha}$, and $G \subset D$. Let $\mathbf{K} : L_2(\partial G) \to L_2(\partial D)$ be the operator defined in (15). Then the range of $\mathbf{K}$ is dense in $L_2(\partial D)$.*

Before proving the theorem, we observe it states that

$$\overline{R(\mathbf{K})} = L_2(\partial D), \tag{17}$$

where $R(\mathbf{K})$ denotes the range of $\mathbf{K}$ and the overbar denotes set closure in $L_2(\partial D)$. It equivalently states that we can find a $g(y) \in L_2(\partial G)$ such that

$$\|(\mathbf{K}g)(x) - f(x)\| < \epsilon, \tag{18}$$

for any given $\epsilon > 0$ and $f(x) \in L_2(\partial D)$, where $\|\cdot\|$ denotes the $L_2(\partial D)$-norm.

Proof of Theorem 1. The equivalence of (17) and (18) follows from the definition of closure. Let $\mathbf{K}^* : L_2(\partial D) \to L_2(\partial G)$ denote the adjoint operator of $\mathbf{K}$ [$\mathbf{K}^*$ exists because $\mathbf{K}$ is defined on the entire space $L_2(\partial G)$]. For any linear and bounded Hilbert-space operator $\mathbf{K}$, it is true (p. 320 of [24]) that

$$\overline{R(\mathbf{K})} = \left[N\left(\mathbf{K}^*\right)\right]^{\perp}, \tag{19}$$

where $N(\cdot)$ denotes the nullspace of an operator and the superscript $\perp$ denotes the orthogonal complement in $L_2(\partial D)$. Because the orthogonal complement of $\{0\}$ is the entire space $L_2(\partial D)$, instead of (17) it suffices to prove that

$$N\left(\mathbf{K}^*\right) = \{0\}. \tag{20}$$

Showing (20) is, in turn, tantamount to demonstrating that the assumption

$$\int_{\partial D} J_0^*(k|x-y|)\, v(x)\, \mathrm{d}s_x = 0, \quad y \in \partial G, \quad v(x) \in L_2(\partial D) \tag{21}$$

leads to the conclusion $v(x) = 0$ almost everywhere on ∂D. In (21), where the superscript $*$ denotes the complex conjugate of a function, we used the well-known expression (p. 354 of [24]) for the adjoint of a Hilbert–Schmidt integral operator.

Let us extend the function on the left-hand side of (21) by assuming that k is the wavenumber of the entire space $\mathbb{R}^2$, allowing y to be arbitrary, and defining

$$w(y) = \int_{\partial D} J_0^*(k|x-y|)\, v(x)\, \mathrm{d}s_x, \quad y \in \mathbb{R}^2. \tag{22}$$

The function $w(y)$ is continuous for any L_2-function $v(x)$. Since $J_0^*(k|x-y|)$ satisfies the complex conjugate of the Helmholtz equation and since we can differentiate (22) under the integral sign, we see that $w(y)$ everywhere satisfies the same equation, viz.,

$$\Delta w(y) + \left(k^*\right)^2 w(y) = 0, \quad y \in \mathbb{R}^2. \tag{23}$$

Written in terms of $w(y)$, our hypothesis (21) is

$$w(y) = 0, \quad y \in \partial G. \tag{24}$$

Eq. (23) is satisfied, in particular, in the open and bounded region G. The interior boundary-value problem consisting of (23) and (24) has the solution $w(y) = 0$. Since (in Section 3) we assumed that ∂G is non-resonant, Section 2.2 tells us that this is the unique continuous solution.

Now any continuous solution to the Helmholtz equation that vanishes in an open subset of $\mathbb{R}^2$ must vanish identically (p. 72 of [18]). Therefore $w(y) = 0$ for all $y \in \mathbb{R}^2$. By the definition (22), this means

$$\int_{\partial D} J_0^*(k|x-y|)\, v(x)\, \mathrm{d}s_x = 0, \quad y \in \mathbb{R}^2. \tag{25}$$

Thus, (21) has now been shown to hold everywhere.

In the special case where y lies on a circle of arbitrary radius a, (25) and (2) give

$$\sum_{m=-\infty}^{\infty} J_m^*(ka) e^{-\mathrm{i}m\phi_y} \int_{\partial D} J_m^*(kr_x) e^{\mathrm{i}m\phi_x} v(r_x, \phi_x)\, \mathrm{d}s_x = 0, \quad 0 \le \phi_y < 2\pi, \tag{26}$$

where (r_x, ϕ_x) and (a, ϕ_y) are the polar coordinates of x and y, respectively, and where $v(r_x, \phi_x)$ denotes $v(x)$. If we further assume that a is such that

$$J_m(ka) \neq 0, \quad m \in \mathbb{N}, \tag{27}$$

then the Fourier series in (26) can be zero only if

$$\int_{\partial D} J_m^*(kr_x) e^{\mathrm{i}m\phi_x} v(r_x, \phi_x)\, \mathrm{d}s_x = 0, \quad m \in \mathbb{N} \cup \{0\}. \tag{28}$$

Consider a circular disc C of sufficiently large radius b; more precisely, require that $C \supset D$ and that $b > r_x$ for all points (r_x, ϕ_x) on ∂D. Suppose that (b, ϕ_y) are the polar coordinates of any point y on the circle ∂C. Multiply (28) by $H_m^{(1)*}(kb) e^{-\mathrm{i}m\phi_y}$ and sum with respect to m to obtain

$$\sum_{m=-\infty}^{\infty} H_m^{(1)*}(kb) e^{-\mathrm{i}m\phi_y} \int_{\partial D} J_m^*(kr_x) e^{\mathrm{i}m\phi_x} v(r_x, \phi_x)\, \mathrm{d}s_x = 0, \quad 0 \le \phi_y < 2\pi. \tag{29}$$

As $b > r_x$, we can use the addition theorem (1) and then take the complex conjugate to get

$$\frac{\mathrm{i}}{4} \int_{\partial D} H_0^{(1)}(k|x-y|)\, v^*(x)\, \mathrm{d}s_x = 0, \quad y \in \partial C, \tag{30}$$

where the factor $\frac{\mathrm{i}}{4}$ is chosen for convenience and where we re-introduced the notation $v(x)$ [for $v(r_x, \phi_x)$].

We now extend the function on the left-hand side of (30) to the interior and exterior of the circle ∂C. We denote the new function by $q(y)$, so that

$$q(y) = \frac{\mathrm{i}}{4} \int_{\partial D} H_0^{(1)}(k|x-y|)\, v^*(x)\, \mathrm{d}s_x, \quad y \in \mathbb{R}^2. \tag{31}$$

The function $q(y)$ is readily recognized (see Section 2.3) as the single-layer potential with density $v^*(x)$. By Section 2.3(iv), $q(y)$ is continuous across ∂D. Re-written in terms of $q(y)$, (30) is the boundary condition

$$q(y) = 0, \quad y \in \partial C. \tag{32}$$

By Section 2.3(ii), $q(y)$ satisfies the Helmholtz equation at all points exterior to ∂D and, in particular, at all points exterior to the disc C (recall that $D \subset C$). Furthermore, $q(y)$ satisfies the Sommerfeld radiation condition at $y = \infty$. As $q(y)$ also satisfies the boundary condition (32), by uniqueness of continuous solutions to the exterior Dirichlet problem (Section 2.2) we have

$$q(y) = 0, \quad y \in \mathbb{R}^2 \setminus \overline{C}. \tag{33}$$

By Section 2.3(iii) (i.e., analyticity), Eq. (33) can be extended to all points $y \in \mathbb{R}^2 \setminus \overline{D}$. By Section 2.3(iv) (i.e., continuity), it then follows that

$$q(y) = 0, \quad y \in \partial D. \tag{34}$$

We now regard (34) as a boundary condition for the interior problem: By Section 2.3(i), the fact that ∂D is nonresonant (Section 3), and uniqueness of continuous solutions to the interior Dirichlet problem (Section 2.2), we have $q(y) = 0$ for $y \in D$. We have thus shown

$$q(y) = 0, \quad y \in \mathbb{R}^2. \tag{35}$$

Finally, analyticity and the jump relation (Section 2.3(iii) and (v)) imply that the single-layer potential $q(y)$ has a density $v(x)$ that is zero almost everywhere on ∂D, which is the desired conclusion. This completes our proof of (17). □

5. Discrete version of MIASS-C: Completeness

Let $\{y_1, y_2, \ldots\}$ be a countable and dense set of points on ∂G. Proceeding from the fact that the operator $\mathbf{K}$ of Section 4 is dense, we show that the discrete system of source-sinks

$$\{J_0\left(k|x - y_m|\right),\ m = 1, 2, \ldots\}, \quad x \in \partial D, \tag{36}$$

is complete in the sense that there exists a finite subset that can generate the boundary data $f(x)$ as closely as we desire. More precisely, we prove the following theorem.

Theorem 2. *Let G and D be non-resonant regions of $\mathbb{R}^2$ with $\partial G \in C^{2,\alpha}$, $\partial D \in C^{2,\alpha}$, and $G \subset D$. Let $\{y_1, y_2, \ldots\}$ be a countable and dense set of points on ∂G, so that $\overline{\{y_1, y_2, \ldots\}} = \partial G$. For any given $\epsilon > 0$ and $f(x) \in L_2(\partial D)$, there exist $n \in \mathbb{N}$ and $\alpha_1, \alpha_2, \ldots, \alpha_n \in \mathbb{C}$ such that*

$$\left\| \sum_{m=1}^{n} \alpha_m J_0\left(k|x - y_m|\right) - f(x) \right\| < \epsilon, \tag{37}$$

where $\|\cdot\|$ denotes the $L_2(\partial D)$-norm.

Proof. By Theorem 1 [more precisely, by its equivalent reformulation in (18)], we can find a $g(y) \in L_2(\partial G)$ such that

$$\left\| \int_{\partial G} J_0\left(k|x - y|\right) g(y)\, \mathrm{d}s_y - f(x) \right\| < \frac{\epsilon}{2}, \tag{38}$$

where we used the explicit expression for $(\mathbf{K}g)(x)$ provided in (15). For the integral appearing in (38), choose any quadrature rule whose quadrature points are the given points $y_1, y_2, \ldots, y_n$, and let $\alpha_1, \alpha_2, \ldots, \alpha_n$ be the corresponding quadrature weights. As long as our quadrature rule is convergent, we can find an n such that

$$\left\| \int_{\partial G} J_0\left(k|x - y|\right) g(y)\, \mathrm{d}s_y - \sum_{m=1}^{n} \alpha_m J_0\left(k|x - y_m|\right) \right\| < \frac{\epsilon}{2}. \tag{39}$$

The desired inequality (37) now follows from (38), (39), and the triangle inequality. □

6. Discrete version of MIASS-C: Linear independence

In Section 5, we saw that the set in (36), (i.e., the system of source-sinks) is complete. We now prove a theorem of linear independence for that set. By the definition of a linearly-independent, countably-infinite set, this amounts to showing that any finite subset is linearly independent:

Theorem 3. *Let G and D be non-resonant regions of $\mathbb{R}^2$ with $\partial G \in C^{2,\alpha}$, $\partial D \in C^{2,\alpha}$, and $G \subset D$. Let $y_1, y_2, \ldots, y_n$ be n discrete points on ∂G. Then*

$$\sum_{m=1}^{n} c_m J_0(k|x - y_m|) = 0 \quad \text{for all } x \in \partial D \implies c_1 = c_2 = \cdots = c_n = 0. \tag{40}$$

Proof. Our proof is analogous to that of Theorem 1: Eq. (40) can be considered as a discrete analog of (21) (the roles of ∂G and ∂D, as well as the roles of x and y are interchanged, and there is no complex conjugate arising from an adjoint). Reasoning as we did in Section 4, we define an extended function

$$w_n(x) = \sum_{m=1}^{n} c_m J_0(k|x - y_m|), \quad x \in \mathbb{R}^2, \tag{41}$$

so that our hypothesis in (40) is

$$w_n(x) = 0, \quad x \in \partial D. \tag{42}$$

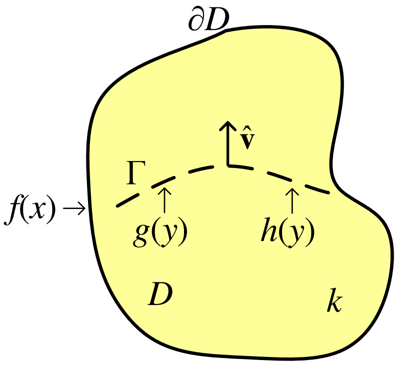

Fig. 2. The considered 2-D interior Dirichlet problem. Shown are the physical closed curve ∂D together with an auxiliary open curve Γ used for the application of MIASS-O.

The steps that gave (35) here lead to

$$q_n(x) = \frac{\mathrm{i}}{4}\sum_{m=1}^{n} c_m H_0^{(1)}(k|x-y_m|) = 0, \quad x \in \mathbb{R}^2. \tag{43}$$

Now allow x to approach any point y_p, where $p \in \{1, 2, \dots, n\}$. The corresponding function $H_0^{(1)}(k|x-y_p|)$ grows without limit, while the rest of the functions $H_0^{(1)}(k|x-y_m|)$ remain finite. Since the sum in (43) is zero, we must have $c_p = 0$. We have thus shown the desired conclusion $c_1 = c_2 = \cdots = c_n = 0$, meaning that (36) is a linearly independent set. □

Remark. The points $y_1, y_2, \dots, y_n \in \partial G$ of Theorem 3 are meant to stand for any n points within the dense set appearing in (36). In other words, our statement of Theorem 3 keeps the same numbering of points as in (36), but actually remains valid for any permutation of the points $y_1, y_2, \dots, y_n$ in (36).

7. Modifications for an open auxiliary curve; MIASS-O

This section concerns MIASS-O, which is our second version of MIASS. MIASS-O is obtained by modifying MIASS-C in two ways, as illustrated in Fig. 2:
(i) We replace the auxiliary closed curve ∂G by an open curve Γ;
(ii) We seek the solution as a superposition of source-sinks and source–sink derivatives, i.e., derivatives in the direction normal to Γ. This amounts to looking for two unknown densities – which we call $g(y)$ and $h(y)$ – instead of only one (namely, the $g(y)$ of Section 3.1).

More specifically, let $\Gamma \in C^{2,\alpha}$ be an open curve lying entirely within D and let $(g(y), h(y)) \in L_2(\Gamma) \times L_2(\Gamma)$ be a *density pair*. Similarly to (12), define the function $u_{g,h}(x)$ by means of the line integral

$$u_{g,h}(x) = \int_{\Gamma}\left[g(y)J_0(k|x-y|) + h(y)\frac{\partial}{\partial \nu}J_0(k|x-y|)\right]\mathrm{d}s_y, \quad x \in D, \tag{44}$$

where $\frac{\partial}{\partial \nu} = \frac{\partial}{\partial \nu(y)}$ denotes the normal to Γ derivative at any point $y \in \Gamma$ (throughout this section, the two endpoints of Γ are tacitly excluded), see Fig. 2. The continuous function $u_{g,h}(x)$ satisfies the Helmholtz equation. Satisfaction of the boundary condition (7) amounts to finding a pair $(g(y), h(y))$ such that

$$\int_{\Gamma}\left[g(y)J_0(k|x-y|) + h(y)\frac{\partial}{\partial \nu}J_0(k|x-y|)\right]\mathrm{d}s_y = f(x), \quad x \in \partial D. \tag{45}$$

We denote by $\mathbf{L} : L_2(\Gamma) \times L_2(\Gamma) \to L_2(\partial D)$ the linear and compact operator associated with the left-hand side of (45), viz.,

$$(\mathbf{L}(g, h))(x) = \int_{\Gamma}\left[g(y)J_0(k|x-y|) + h(y)\frac{\partial}{\partial \nu}J_0(k|x-y|)\right]\mathrm{d}s_y. \tag{46}$$

The operator $\mathbf{L}$, whose range belongs to the boundary ∂D, is analogous to the $\mathbf{K}$ of Section 3.2.

7.1. Density of range

The theorem that follows states that $\mathbf{L}$ has a dense range and directly corresponds to Theorem 1. The proof is similar to that of Theorem 1 in that the adjoint operator is involved; but the homogeneous boundary-value problem associated with the adjoint operator is Cauchy rather than Dirichlet.

Theorem 4. *Let D be a non-resonant region of $\mathbb{R}^2$ with $\partial D \in C^{2,\alpha}$, and let $\Gamma \in C^{2,\alpha}$ be an open curve with $\Gamma \subset D$. Let $\mathbf{L} : L_2(\Gamma) \times L_2(\Gamma) \to L_2(\partial D)$ be the operator defined in (46). Then the range of $\mathbf{L}$ is dense in $L_2(\partial D)$.*

Proof. By analogy to (20), it suffices to show that

$$N\left(\mathbf{L}^*\right) = \{0\}, \tag{47}$$

where $\mathbf{L}^* : L_2(\partial D) \to L_2(\Gamma) \times L_2(\Gamma)$ denotes the adjoint of $\mathbf{L}$. This time, we must show that the pair of assumptions

$$\int_{\partial D} v(x) J_0^*(k|x-y|)\, \mathrm{d}s_x = 0, \quad y \in \Gamma, \quad v(x) \in L_2(\partial D) \tag{48}$$

and

$$\int_{\partial D} v(x) \frac{\partial}{\partial \nu} J_0^*(k|x-y|)\, \mathrm{d}s_x = 0, \quad y \in \Gamma, \quad v(x) \in L_2(\partial D) \tag{49}$$

leads to the conclusion $v(x) = 0$ almost everywhere on ∂D.

We extend the function on the left-hand side of (48) by allowing y to be arbitrary and defining

$$w(y) = \int_{\partial D} v(x) J_0^*(k|x-y|)\, \mathrm{d}s_x, \quad y \in \mathbb{R}^2, \tag{50}$$

which is a continuous function that everywhere satisfies the complex conjugate of the Helmholtz equation, viz.,

$$\Delta w(y) + \left(k^*\right)^2 w(y) = 0, \quad y \in \mathbb{R}^2. \tag{51}$$

Written in terms of $w(y)$, our two hypotheses (48) and (49) amount to

$$w(y) = \frac{\partial}{\partial \nu} w(y) = 0, \quad y \in \Gamma. \tag{52}$$

Together, Eqs. (51) and (52) form a homogeneous Cauchy problem for the Helmholtz equation [24] which, within the open region D, has the unique solution $w(y) = 0$. By analyticity of solutions to the Helmholtz equation, we have $w(y) = 0$ for all $y \in \mathbb{R}^2$. By the definition (50), this means

$$\int_{\partial D} J_0^*(k|x-y|)\, v(x)\, \mathrm{d}s_x = 0, \quad y \in \mathbb{R}^2, \tag{53}$$

which is the same as (25) in the proof of Theorem 1. The remaining parts of that proof hold verbatim so that $\mathbf{L}$ (just like $\mathbf{K}$) has a range that is dense in $L_2(\partial D)$. □

Remark. The assumption of having a non-resonant ∂G (which concerns MIASS-C, see Theorem 1) has no analogy in MIASS-O and Theorem 4.

7.2. Completeness and linear independence

Let $\{y_1, y_2, \ldots\}$ be a countable and dense set of points on Γ. The discrete system to be used in MIASS-O [in place of (36)] is

$$\{J_0(k|x-y_m|),\ m = 1, 2, \ldots\} \cup \{\frac{\partial}{\partial \nu} J_0(k|x-y_m|),\ m = 1, 2, \ldots\}, \quad x \in \partial D, \tag{54}$$

Since $\mathbf{L}$ has a dense range, the proof of Theorem 2 carries over to MIASS-O, so that the system is complete, just like the one in Section 5. The system is also linearly independent, but the proof differs slightly from that in Section 6:

Theorem 5. *Let D be a non-resonant region of $\mathbb{R}^2$ with $\partial D \in C^{2,\alpha}$, and let $\Gamma \in C^{2,\alpha}$ be an open curve with $\Gamma \subset D$. Let $y_1, y_2, \ldots, y_n$ be n discrete points on Γ. Then*

$$\sum_{m=1}^{n} \left[c_m J_0(k|x-y_m|) + d_m \frac{\partial}{\partial \nu} J_0(k|x-y_m|) \right] = 0 \quad \textit{for all } x \in \partial D$$
$$\Longrightarrow\ c_1 = d_1 = c_2 = d_2 = \cdots = c_n = d_n = 0. \tag{55}$$

Proof. We begin as in the proof of Theorem 3. Here, the hypothesis in (55) leads to

$$\sum_{m=1}^{n} \left[c_m H_0^{(1)}(k|x-y_m|) + d_m \frac{\partial}{\partial \nu} H_0^{(1)}(k|x-y_m|) \right] = 0, \quad x \in \mathbb{R}^2. \tag{56}$$

The identity

$$\frac{\partial}{\partial \chi} H_0^{(1)}\left(k\sqrt{\chi^2+\psi^2}\right) = -\frac{k\chi}{\sqrt{\chi^2+\psi^2}} H_1^{(1)}\left(k\sqrt{\chi^2+\psi^2}\right), \quad \chi, \psi \in \mathbb{R} \tag{57}$$

shows that $\frac{\partial}{\partial \nu} H_0^{(1)}(k|x-y_m|)$ tends to zero (or infinity) when x approaches y_m from the normal (or tangential) to Γ direction, respectively.

In (56), allowing x to approach any y_p from the normal to Γ direction results in exactly one unbounded term, namely $c_p H_0^{(1)}(k|x-y_p|)$ [all other terms remain bounded; in particular, (57) shows that $\frac{\partial}{\partial \nu} H_0^{(1)}(k|x-y_p|)$ approaches zero]. The fact that the sum in (56) equals zero then implies $c_p = 0$, so that $c_1 = c_2 = \cdots = c_n = 0$. Repeating this process – but approaching each y_p from the tangential direction – leads to the further conclusion $d_1 = d_2 = \cdots = d_n = 0$. □

8. Implementation of MIASS; numerical results for elliptical cavity

To solve a given interior Dirichlet problem within a closed region D, we first choose a finite set of points, say $\{y_1, y_2, \ldots, y_n\}$, located on the auxiliary curve, namely the closed curve ∂G when applying MIASS-C (cf. (36)), or the open curve Γ in the case of MIASS-O (cf. (54)). Consequently, there are n unknowns in the case of MIASS-C, namely the coefficients of the source-sinks/Bessel functions; and $2n$ unknowns in the case of MIASS-O, i.e. the coefficients of the source-sinks together with those of the source–sink derivatives.

We then require our functions to approximately generate the continuous boundary data $f(x)$ on ∂D. A straightforward way of doing this is to sample the data at a number of matching points on ∂D equal to the number of unknowns, leading to a square matrix ($n \times n$ for MIASS-C or $(2n) \times (2n)$ for MIASS-O) for the resulting system of linear equations. Another straightforward way is to sample the data at N matching points on ∂D, where N is larger than the number (n or $2n$) of unknowns. We have found that this second choice may be quite beneficial from the point of view of numerics, an issue we plan to discuss in more detail in a future paper.

In what follows, we show indicative numerical results using a square matrix ($n \times n$) for MAS and MIASS-C and a rectangular matrix $[N \times (2n)$, where $N \geq 2n]$ for MIASS-O. Note that, in the case of MIASS-O, the discrete-sources number is equal to twice the number of source-sinks and, also, to twice the number of source–sink derivatives.

In the case of MIASS-C, the square matrix is

$$[J_0(k|x_l - y_m|)], \quad l, m = 1, \ldots, n. \tag{58}$$

Solving the $n \times n$ system yields the source–sink coefficients, which are denoted in this paper by $I_1, I_2, \ldots, I_n$ (this notation facilitates a comparison with the MAS numerical results of [23]). Finally, the superposition

$$u_n^C(x) = \sum_{m=1}^{n} I_m J_0(k|x-y_m|) \tag{59}$$

gives the approximate solution of our boundary-value problem obtained via MIASS-C.

The procedure of MIASS-C just described amounts to two changes in the $n \times n$ system of the conventional MAS, namely the replacement of the exterior to ∂D auxiliary curve by an interior one and, also, to the replacement – in both (58) and (59) – of the Hankel functions $H_0^{(1)}$ by Bessel functions J_0.

In the case of MIASS-O, the rectangular matrix of the aforementioned overdetermined system is given by

$$\left[J_0(k|x_l - y_m|) \left| \frac{\partial}{\partial \nu} J_0(k|x_l - y_m|) \right. \right], \quad l = 1, \ldots, N, \quad m = 1, \ldots, n \tag{60}$$

where $N > 2n$. The equation corresponding to (59) is

$$u_n^O(x) = \sum_{m=1}^{n} \left[I_m J_0(k|x-y_m|) + \tilde{I}_m \frac{\partial}{\partial \nu} J_0(k|x-y_m|) \right]. \tag{61}$$

We now implement these two procedures, and present numerical results, for the case where ∂D is an ellipse with semi-axes a and b. In the case of MIASS-C, the internal closed auxiliary curve ∂G is also an ellipse with semi-axes σa and σb, where the scale factor σ satisfies $0 < \sigma < 1$, ensuring $G \subset D$. The ellipses ∂D and ∂G are similar and have the same eccentricity $e = \sqrt{1-(b/a)^2}$. The points x_l along ∂D are chosen as follows: With ∂D described by the standard 2π-periodic parametric representation,

$$x(t) = (\chi(t), \psi(t)) \in \mathbb{R}^2, \qquad \chi(t) = a\cos t, \qquad \psi(t) = b \sin t, \quad 0 \leq t \leq 2\pi \tag{62}$$

(so that χ and ψ are the coordinates along the major- and minor-semi-axes, respectively), our choice of points x_l is

$$x_l = \left(\chi\left(\frac{2\pi l}{n}\right), \psi\left(\frac{2\pi l}{n}\right) \right) \in \mathbb{R}^2, \quad l = 1, 2, \ldots, n. \tag{63}$$

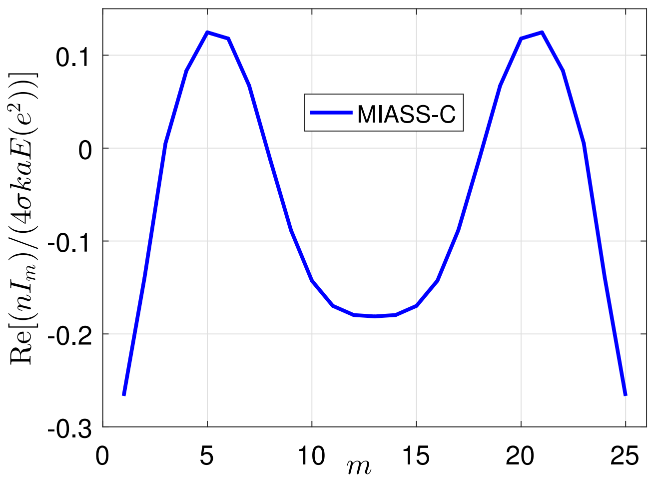

(a)

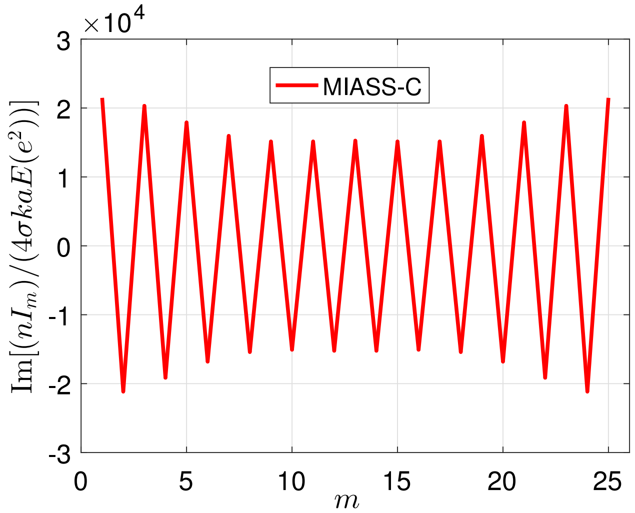

(b)

Fig. 3. Real (a) and imaginary (b) parts of the normalized MIASS-C auxiliary-source coefficients $nI_m/(4\sigma kaE(e^2))$ (E is the complete elliptic integral of the second kind) versus m; $ka = 5$, $kb = 4.3$ ($e = 0.5103$), $kx_{\rm fil} = (3.5, 0)$, $n = 24$, and $\sigma = 0.9$. The last point (corresponding to $m = 25 = n + 1$, and equaling the first point) is included for reasons of symmetry.

Our points y_m are given by an analogous formula. To facilitate a comparison with [23], we take $f(x)$ to be the velocity potential generated by a line source (filament) located at $x_{\rm fil} = (\chi_{\rm fil}, 0) \in \mathbb{R}^2$ and generating the primary field $H_0^{(1)}(k|x - x_{\rm fil}|)$.

For the case $ka = 5$, $kb = 4.3$ ($e = 0.5103$), $\sigma = 0.9$, $kx_{\rm fil} = (3.5, 0)$, and $n = 24$, the real and imaginary parts of the intermediary quantities I_m are shown in Figs. 3(a) and 3(b). We have normalized our results consistently with [25]. We observe that

(i) the imaginary parts $\mathrm{Im}\{I_m\}$ are much larger than the real parts $\mathrm{Re}\{I_m\}$;

(ii) the imaginary parts oscillate (i.e., imaginary parts of adjacent I_m have opposite signs and alternate between large positive and negative values).

In the case of MIASS-O, the open auxiliary curve Γ is a line segment on the χ-axis hosting $2n = 26$ functions in total, namely $n = 13$ source-sinks/Bessel functions and $n = 13$ source–sink derivatives. The real and imaginary parts of I_m and $\tilde{I}_m$ (for the same elliptical physical boundary ∂D) are depicted in Figs. 4(a), 4(b) and 5(a), 5(b), respectively. Both I_m and $\tilde{I}_m$ behave in a manner similar to the I_m of MIASS-C (see points (i) and (ii) above). Additionally, with the single exception of $\mathrm{Re}\{I_3\}$ ($m = 3$), all values of $\mathrm{Re}\{I_m\}$ and $\mathrm{Re}\{\tilde{I}_m\}$ are very small.

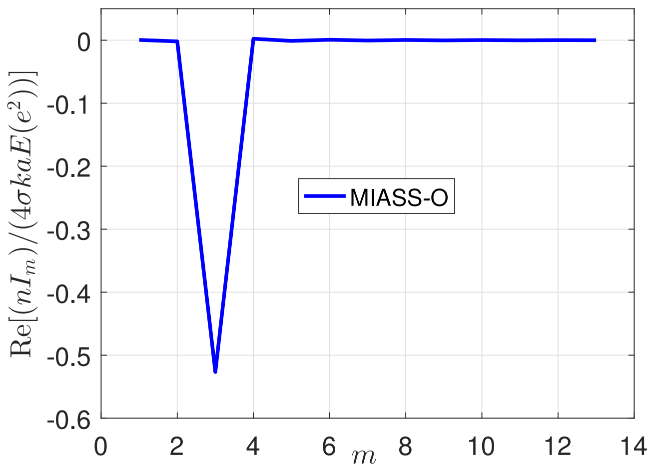

(a)

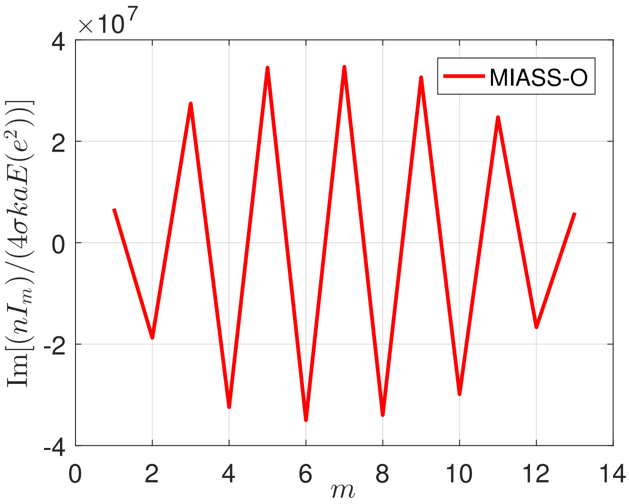

(b)

Fig. 4. Like Fig. 3, but results obtained using MIASS-O with $n = 13$.

Oscillations in I_m are also present in the conventional MAS. For the case of internal Dirichlet problems involving circular discs, this phenomenon is discussed in detail in [23] (see also [25] for extensions to more complicated shapes). Consequently, the undesirable phenomenon of oscillations in the MAS continues to manifest itself in both MIASS-C and MIASS-O.

Numerical results, however, indicate that the oscillatory behaviors are fundamentally different. Figs. 6(a) and 6(b) are corresponding figures for the case of conventional MAS. Two differences are apparent: Firstly, in MAS oscillations occur in the real part rather than in the imaginary part. Secondly (and more importantly) oscillations occur mainly for small and large values of m, corresponding to those auxiliary sources that are closer to the primary excitation (which is on the χ-axis). In MIASS, by contrast, *all* I_m oscillate. For our MAS results in Fig. 6, we chose the values of n and σ ($\sigma > 1$ in the case of MAS) so as to obtain roughly the same matrix (2-norm) condition number as in MIASS-C (where a square linear system is involved). Both condition numbers are of the order of 10^{10}, which is large but manageable for most existing computational platforms. For the present computations, we used the MATLAB R2019a® programming language and obtained the same results by using different numerical solvers. We thus concluded that, for the considered parameter values, no roundoff/matrix ill-conditioning effects are encountered.

For the case of MAS and MIASS-C, we further calculated the associated boundary errors, i.e., the velocity potential $v_n(x)$ on the boundary minus the given boundary data, which is theoretically supposed to be zero. As expected, one sees very

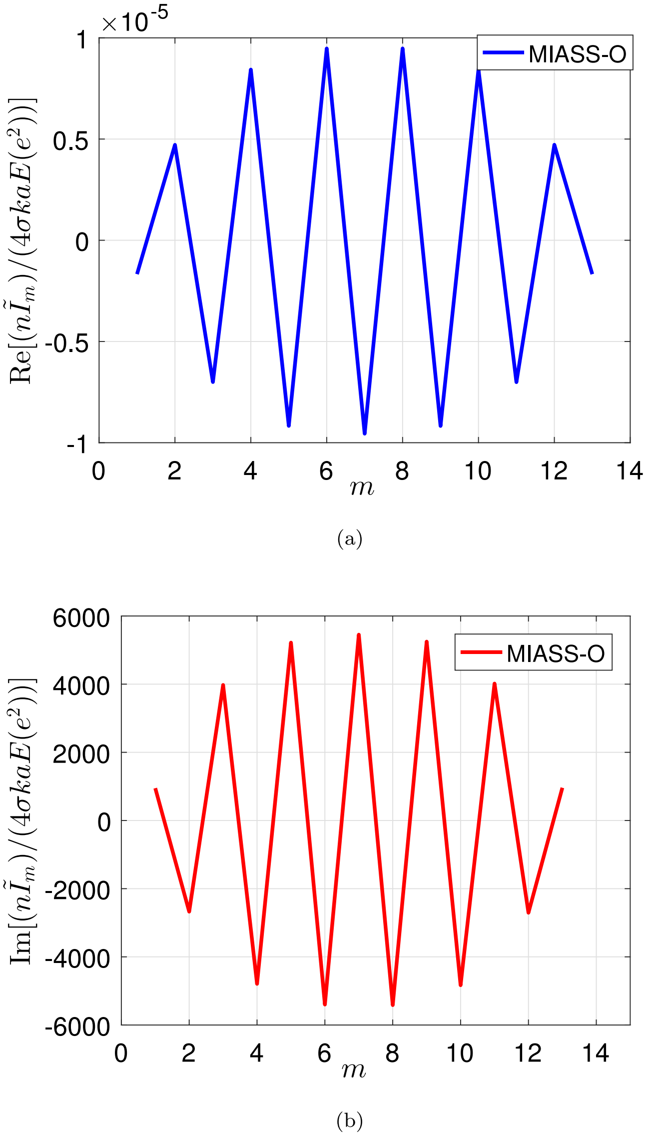

Fig. 5. Like Fig. 3, but results obtained using MIASS-O with $n = 13$.

small (of the order of 10^{-12} to 10^{-13}) and noisy values. Thus, these results independently support the aforementioned conclusion that the large condition numbers are unimportant. Furthermore, MIASS-C gives values of the same order of magnitude with MAS, even if, in MIASS-C, the value of n is smaller (24 vs. 64).

While the aforementioned boundary errors demonstrate an advantage of MIASS-C over MAS for the particular case studied, the aforementioned comparisons between MAS, MIASS-C and MIASS-O should be considered preliminary. A fair comparison should, among other factors, take into account: the particular given boundary data (if, for example, the data is generated by a line source, it is known from [23] that the position of the line source greatly affects the oscillations and the condition numbers in the MAS); the placement and number of the matching points, especially when the boundary ∂D is not smooth; the position and shape of the various auxiliary curves; our remark concerning the number of matching points vs. the number of discrete-source points, etc. We have certainly not made optimum choices and depending on the problem, each method can be expected to have its own advantages and drawbacks.

We finally turn to the velocity potential $u_n(x)$. Figs. 7(a) and 7(b) compares the MIASS-C, MIASS-O and MAS results at observation points lying on an ellipse with a scale factor $\sigma = 0.8$. At the scale of Figs. 7(a) and 7(b), the three sets of results coincide. Thus, despite the oscillations and the large condition numbers, we obtain the same results. Via additional

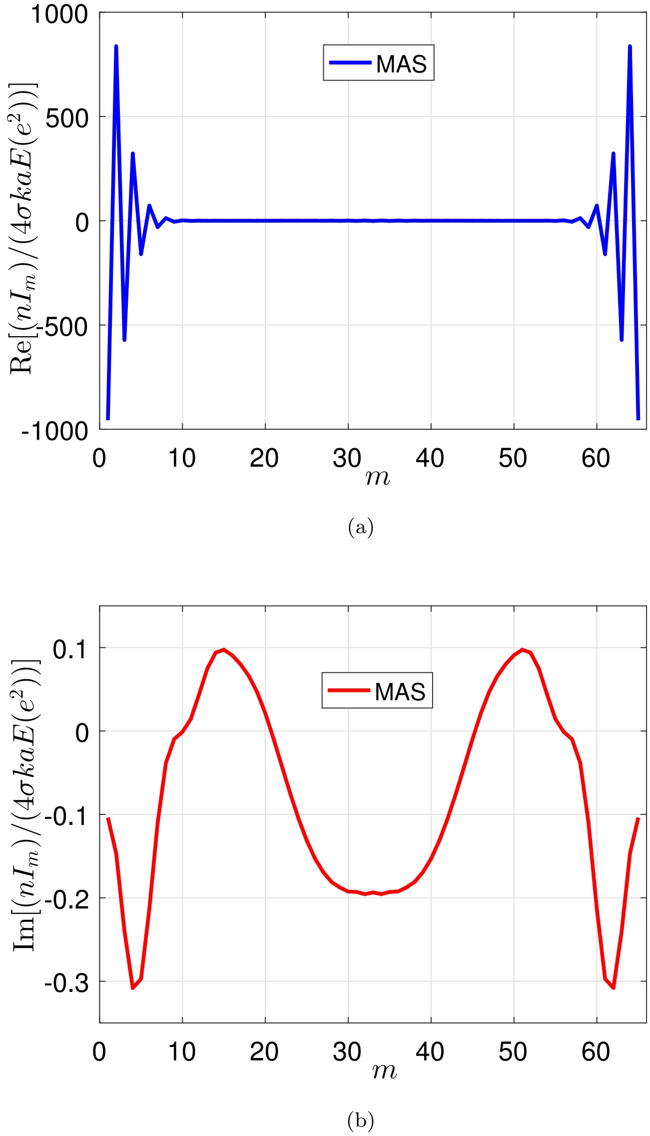

Fig. 6. Like Fig. 3, but results obtained using MAS with $n = 64$ and $\sigma = 2$.

extensive numerical tests, we found that this was always true (except for cases where the condition numbers become prohibitively large).

9. Future work

This work discussed fundamental aspects of two versions (MIASS-C and MIASS-O) of the Method of Internal Auxiliary Source–Sinks (MIASS), including the relations of MIASS to other methods, especially to the Method of Auxiliary Sources (MAS). We believe that MIASS (or extensions) will prove useful for a number of problems involving interior regions. Future work will include:

(i) Extensions of both versions of MIASS to the 2-D transmission problem, including proofs of completeness and linear independence.

(ii) More detailed studies of the oscillatory behavior discussed in Section 8. For the case of MAS, [23] carries out such studies by *analytically* examining the MAS solution for the simple case where ∂D and ∂G are circular discs. These studies (see also ch. 5 of [1], which refers to exterior problems) help us better understand more complicated geometries [25]. Preliminary findings indicate that the methods of [23] carry over to the case of MIASS-C, facilitating more detailed comparisons of MIASS-C to MAS.

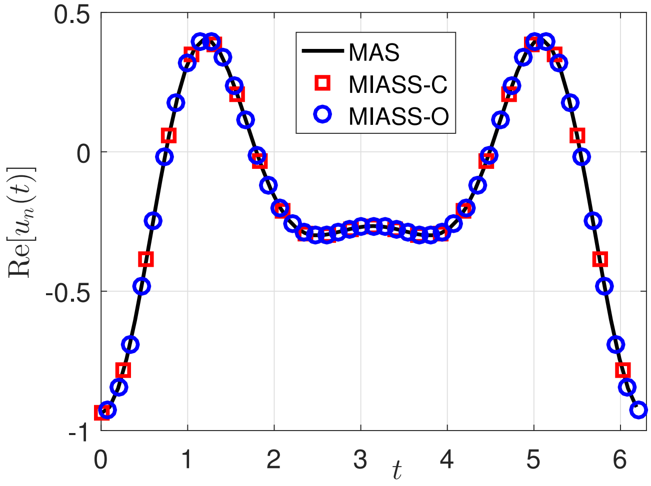

(a)

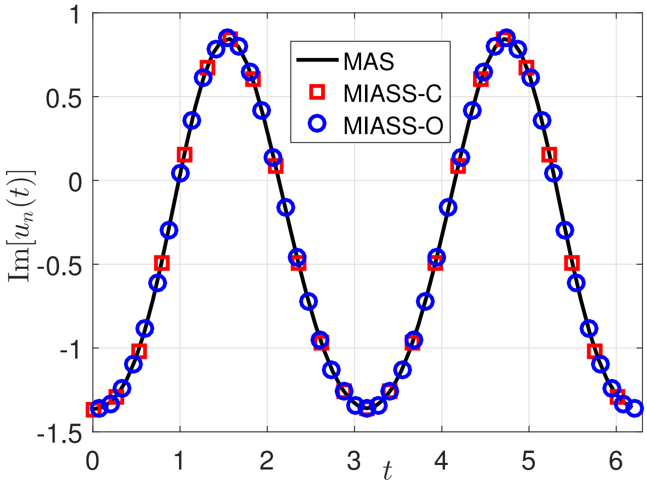

(b)

Fig. 7. Real (a) and imaginary (b) acoustic field $u_n(x)$ computed from the I_m of Figs. 3, 4, 5, and 6 at observation points x lying on an ellipse with $\sigma = 0.8$. Results are shown as a function of t, which is the parameter in (62).

Acknowledgment

We gratefully acknowledge the German Academic Exchange Service (DAAD) program PPP Griechenland 2018 "Studies on generalized multipole techniques and the method of auxiliary sources, with applications to electron energy loss spectroscopy".

References

[1] T. Wriedt, Y. Eremin, The Generalized Multipole Technique for Light Scattering, Springer, 2018.

[2] O.A. Sapozhnikov, An exact solution to the Helmholtz equation for a quasi-Gaussian beam in the form of a superposition of two sources and sinks with complex coordinates, Acoust. Phys. 58 (1) (2012) 41–47 (original Russian text published in Akusticheskii Zhurnal, 2012, 58 (1) 49–56).

[3] C.J.R. Sheppard, S. Saghafi, Beam modes beyond the paraxial approximation: A scalar treatment, Phys. Rev. A 57 (4) (1998) 2972–2979.

[4] V.D. Kupradze, On the approximate solution of problems in mathematical physics, Russian Math. Surveys 22 (2) (1967) 58–108 (in English).

[5] A. Doicu, Y. Eremin, T. Wriedt, Acoustic and Electromagnetic Scattering Analysis using Discrete Sources, Academic Press, London, UK, 2000.

[6] D. Colton, Runge's theorem and far field patterns for the impedance boundary value problem in acoustic wave propagation, SIAM J. Math. Anal. 13 (6) (1982) 970–977.

[7] R.F. Millar, On the completeness of sets of solutions to the Helmholtz equation, IMA J. Appl. Math. 30 (1983) 27–37.
[8] Y.A. Eremin, A.G. Sveshnikov, The Discrete Sources Method in Electromagnetic Diffraction Problems, Moscow State University Press, Moscow, 1992 (in Russian).
[9] Y.A. Eremin, A.G. Sveshnikov, Discrete sources method in electromagnetic scattering problems, Electromagnetics 13 (2) (1993) 203–215.
[10] A.G. Sveshnikov, Yu. A. Eremin, Numerical analysis of scattering problems on the bodies of revolution by non-orthogonal series method, Izv. Vyssh. Uchebn. Zaved. Radiofiz. 23 (8) (1980) 1006–1008 (in Russian).
[11] A.G. Sveshnikov, Yu. A. Eremin, Extension of non-orthogonal series method and analysis of scattering problems on the penetrable bodies, Izv. Vyssh. Uchebn. Zaved. Radiofiz. 25 (5) (1982) 580–583 (in Russian).
[12] Yu. A. Eremin, A.G. Sveshnikov, Substaintiation of the method of non-orthogonal series and solution of some converse problems in diffraction, USSR Comput. Math. Math. Phys. 23 (3) (1983) 142–146.
[13] Yu. A. Eremin, Representation of fields in terms of sources in the complex plane in the method of nonorthogonal series, Sov. Phys. Dokl. 28 (6) (1983) 451–452.
[14] Yu. A. Eremin, A.G. Sveshnikov, Scattering problems analysis on penetrable bodies via multipole sources method, Izv. Vyssh. Uchebn. Zaved. Radiofiz. 28 (5) (1985) 647–653 (in Russian).
[15] Yu. A. Eremin, Complete system of functions for the study of boundary value problems in mathematical physics, Sov. Phys. Dokl. 32 (8) (1987) 635–637.
[16] Yu. A. Eremin, N.V. Orlov, A.G. Sveshnikov, Modified method of multipole sources in the problems of diffraction of electromagnetic waves, J. Commun. Technol. Electron. 38 (4) (1993).
[17] Yu. A. Eremin, N.V. Orlov, V.I. Rozenberg, Multiple electromagnetic scattering by a linear array of electrified raindrops, J. Atmos. Terr. Phys. 57 (3) (1995) 311–319.
[18] D. Colton, R. Kress, Integral Equation Methods in Scattering Theory, Krieger Publishing Company, Malabar, Fl, 1992.
[19] D. Colton, R. Kress, Inverse Acoustic and Electromagnetic Scattering Theory, second ed., Springer, 1998.
[20] Staff of the Bateman Manuscript Project (A. Erdélyi (Editor), W. Magnus, F. Oberhettinger, and F.G. Tricomi (Research Associates)), Higher Transcendental Functions, McGraw-Hill, New York, 1953 (Reprinted, Malabar, FL: Robert Krieger Publishing Co. 1981).
[21] F.W.J. Olver, D.W. Lozier, R.F. Boisvert, C.W. Clark, Digital Library of Mathematical Functions, National Institute of Standards and Technology from http://dlmf.nist.gov/.
[22] G. Dassios, R. Kleinman, Low Frequency Scattering, Clarendon Press, Oxford, 2000.
[23] G. Fikioris, O.N. Bakas, G.P. Zouros, Study of convergence divergence and oscillations in Method-of-Auxiliary-Sources (MAS) and Extended-Integral-Equation (EIE) solutions to a simple cavity problem, IEEE Trans. Microw. Theory Tech. 61 (8) (2013) 2773–2782.
[24] I. Stakgold, Green's Functions and Boundary Value Problems, John Wiley, 1979.
[25] N.L. Tsitsas, G.P. Zouros, G. Fikioris, Y. Leviatan, On methods employing auxiliary sources for 2-D electromagnetic scattering by non-circular shapes, IEEE Trans. Antennas and Propagation 66 (10) (2018) 5443–5452.